2024 IEEE International Conference on Robotics and Automation (ICRA 2024)
May 13-17, 2024. Yokohama, Japan

Enhancing Tactile Sensing in Robotics: Dual-Modal Force and Shape Perception with EIT-based Sensors and MM-CNN

Haofeng Chen[1,2], Xuanxuan Yang[1,2], Gang Ma[*2],Yucheng Wang[1], Xiaojie Wang[*1,3]

***Abstract*— Electrical Impedance Tomography (EIT)-based tactile sensors offer durability, scalability, and cost-effective manufacturing. However, simultaneously reconstructing force and shape from boundary measurements remains challenging due to EIT's inherent location dependencies and image artifacts. This study presents a model-driven multimodal convolutional neural network (MM-CNN) for joint EIT-based force and shape sensing. The hybrid approach combines physics-inspired voltage preprocessing with an attention-based network to overcome EIT's limitations. The preprocessing network applies a linearized one-step inverse solution with Tikhonov regularization to convert raw boundary voltage into a noise-reduced 2D image. The image reconstruction network uses an attention mechanism to focus on salient features, addressing location dependency issues. Quantitative metrics show that MM-CNN outperforms traditional EIT algorithms like NOSER and TV, reducing location dependency and improving shape discrimination. MM-CNN enables unified force and shape modalities, validated through real-contact experiments, enhancing EIT tactile systems for human-robot interaction by incorporating physical knowledge with deep learning.**

I. Introduction

Tactile sensing plays a pivotal role in empowering robots to intricately perceive their surroundings and process various stimuli simultaneously, facilitating safe and effective motion even in unstructured environments. Furthermore, robust artificial tactile perception significantly bolsters the environmental awareness crucial for seamless human-robot collaboration, thereby enhancing safety during close interactions [1]–[3].

However, the challenge arises when attempting to scale tactile sensing across extensive surface areas using conventional sensor arrays. These arrays demand high-density sensing units to capture intricate spatial touch information accurately. Unfortunately, this pursuit introduces complications related to scalability, cost-efficiency, and the intricate complexity of data communication within tactile sensor design [4], [5].

Recently, a promising solution has emerged in the form of tactile sensors founded on electrical impedance tomography (EIT). EIT serves as a non-array technology that excels at large-area touch sensing in robotics [5], [6]. The technology is based on nondestructive imaging, where it reconstructs conductivity distributions through sparse boundary electrodes [7]. This reconstruction process encompasses the estimation of touch location, shape, and intensity by translating measurements of voltage responses to applied current stimulations into conductivity images.

In stark contrast to the traditional array-based sensors, EIT-based tactile sensors are crafted as flexible, integrated structures free of discrete internal components. This innovative approach facilitates the creation of a single, integrated sensing surface. As a result, this holistic fabrication methodology provides an efficient, scalable, and cost-effective solution for achieving continuous large-area tactile coverage through EIT-based sensors.

Nonetheless, the application of electrical impedance tomography (EIT) presents inherent mathematical challenges, primarily due to its ill-posed inverse problem. This characteristic inherently limits the fidelity of image reconstruction and the precision of contact shape determination within EIT-based tactile sensors. Furthermore, EIT exhibits location-dependent spatial performance, wherein perception sensitivity varies based on the point of touch [8]. This variability complicates the accurate detection of contact force within EIT tactile systems.

Addressing these limitations has proven to be a challenge for conventional model-driven methods such as NOSER [9] and total variation regularization (TV) [10], primarily due to their constrained modeling capabilities. Recently, the application of machine learning has shown considerable potential in overcoming EIT tactile sensing challenges. Existing EIT-based tactile sensing systems have excelled in either shape detection [11], [12] or force estimation [13].

However, an integrated approach capable of simultaneously achieving high-performance force and shape sensing remains an unsolved problem. While Husain et al. [11] managed to recognize three fundamental shapes using machine learning for solving the EIT inverse problem and image post-processing, they neglected to incorporate force sensing. Similarly, the work of Park et al. [12] introduced a novel neural network that enhanced spatial resolution and shape reconstruction, yet it still lacked the ability to estimate force. In contrast, Lee et al. [13] successfully estimated multi-contact forces through a simulation-assisted mapping pipeline but did not enable shape detection. An all-encompassing methodology that synergistically combines model-based and data-driven techniques is paramount for overcoming these intrinsic limitations.

This paper introduces an innovative EIT-based tactile sensor that revolutionizes the field by enabling dual-force and

Xiaojie Wang(e-mail: xjwang@iamt.ac.cn) Gang Ma (e-mail: magang93@ustc.edu.cn)

[1]Haofeng Chen, Xuanxuan Yang, Yucheng Wang and Xiaojie Wang are with the Institute of Intelligent Machines, Hefei Institutes of Physical Science, Chinese Academy of Sciences, Hefei 230031, China.

[2]Haofeng Chen, Xuanxuan Yang and Gang Ma are with the University of Science and Technology of China, Hefei, Anhui 230026, China.

[3]Xiaojie Wang is with Chongqing University of Posts and Telecommunications,Chongqing 400030, China.

shape sensing modalities through the implementation of a novel model-driven multimodal convolutional neural network (MM-CNN). The proposed MM-CNN entails physics-based voltage preprocessing and an attention-based reconstruction network. By harmoniously integrating the strengths of both model-driven and data-driven techniques, this hybrid approach achieves a breakthrough in unified force and shape sensing. The effectiveness of the sensor is substantiated through quantitative and visual results, showcasing its unparalleled ability to sense both force and shape modalities.

II. METHODS AND SYSTEM DESIGN

Figure 1 (Top) depicts an overview of the proposed MM-CNN network, which is capable of detecting both touch shape and force intensity. It consists of two key components: a pre-processing network and an image reconstruction network. Figure 1 (Bottom) illustrates the full network architecture of the MM-CNN network. The specific designs of the pre-processing and image reconstruction modules are detailed in the following sections.

A. Pre-processing net

The pre-processing network comprises three sequential modules: a pre-reconstructor, a mask layer, and a thresholding module, as illustrated in Figure 1 (Top). In order to transform the boundary voltage into a two-dimensional image, we employed a linearized, one-step inverse solution involving Tikhonov regularization. Subsequently, an obtained one-dimensional conductivity vector is reshaped into a two-dimensional image, denoted as $\mathbf{I}^{pre}$. The progression can be outlined as follows:

$$\mathbf{I}^{pre} = reshape((\mathbf{J}^T\mathbf{W}\mathbf{J} + \lambda^2\mathbf{R})^{-1}\mathbf{J}^T\mathbf{W}\Delta V)) \quad (1)$$

where $reshape(\cdot)$ is the reshape operator, $\mathbf{J}^T$ signifies the transpose of sensitivity matrix $\mathbf{J}$ [14], λ is a regularization hyperparameter value. In this study, we used a moderate hyperparameter λ=0.15 to balance image quality and stability. $\mathbf{W}$ is the weight of matrix, and $\mathbf{R}$ is regularization matrix [15]. Additionally, $\mathbf{RM} = (\mathbf{J^T W J} + \lambda^{\mathbf{2}}\mathbf{R})^{-\mathbf{1}}\mathbf{J^T W}$ denotes reconstruction matrix. The Newton's One-Step Error Reconstructor (NOSER) prior [9] is used for calculating the matrix $\mathbf{R}$. The proposed pre-reconstructor module, derived from (1), provides two key benefits. First, the module integrates physics-based priors, enabling faster training convergence. These informative priors provide regularization, guiding the model toward physically plausible solutions. Second, it transforms the raw voltage measurements into a concise image encoding spatial and structural insights. Specifically, projection onto an image plane captures the essential conductivity distribution in the spatial domain. This representation retains pertinent details, furnishing an informative perspective of the conductivity characteristics.

For the EIT-based tactile sensor in this study, external contact creates local impedance changes that are negative in polarity. However, boundary noise can introduce positive artifacts degrading the reconstruction. To extract only valid negative changes, we implement a mask layer module generating a binary mask $\mathbf{I}^{mask}$ containing this region, denoted as $\mathbf{I}^{mask}$:

$$\mathbf{I}^{mask} = H(\mathbf{I}^{pre}) \quad (2)$$

where $H(\cdot)$ denotes the Heaviside step function, also known as the unit step function.

Then, the valid negative impedance change region is extracted by applying the mask:

$$\mathbf{I}^{mult} = \mathbf{I}^{mask} \odot \mathbf{I}^{pre} \quad (3)$$

where $\odot$ is Hadamard product operator.

Apart from positive conductivity artifacts, reconstructed images may contain spurious negative artifacts deteriorating quality. These stem from noise and inconsistencies. To mitigate this, we implement a thresholding module using a modified ReLU function to remove minor negative artifacts while retaining valid contact-induced changes:

$$\mathbf{I}^{thresh} = \mathrm{MReLU}(\mathbf{I}^{mult}) \quad (4)$$

For a given matrix or vector x, the modified ReLU function $\mathrm{MReLU}(x)$ is defined as:

$$\mathrm{MReLU}(x) = \begin{cases} 0, x < \tau \\ x, x > \tau \end{cases} \quad (5)$$

where $\tau = |t \cdot x_{\arg\max_i |x_i|}|$ is the threshold value determined by the maximum absolute value in x multiplied by a scaling factor t. The value of t is chosen empirically through trials [8], [14].

B. Image reconstruction network

The image reconstruction network architecture is shown in Figure 1 (Bottom). Our prior work [16] used a basic convolutional network prone to EIT's inherent location-dependency. To address this, the proposed MM-CNN incorporates an attention mechanism providing spatial guidance to focus on salient features and suppress unnecessary ones. Specifically, we implement a convolutional block attention module (CBAM) [17] with sequential channel and spatial attention layers for adaptive feature refinement. This boosts performance without substantially increasing complexity.

Additionally, the network employs three convolutional layers for feature extraction followed by four deconvolutional layers for reconstructing the output image. All convolutional and deconvolutional layers use 3×3 filters with stride 1. The max pooling layers are configured with 2×2 filter size and stride 0. For upsampling, we apply 3×3 transposed convolution with stride 1 and an upsampling factor of (2,2) along the rows and columns. ReLU activation is used throughout the network, and batch normalization is applied after each convolutional/deconvolutional layer to improve generalizability and accelerate training.

For optimization, we jointly minimize MSE and MAE loss terms to leverage their complementary advantages. While MSE encourages smooth convergence, MAE reduces the influence of outliers and preserves fine-grained details essential for reconstructing the conductivity peak accurately.

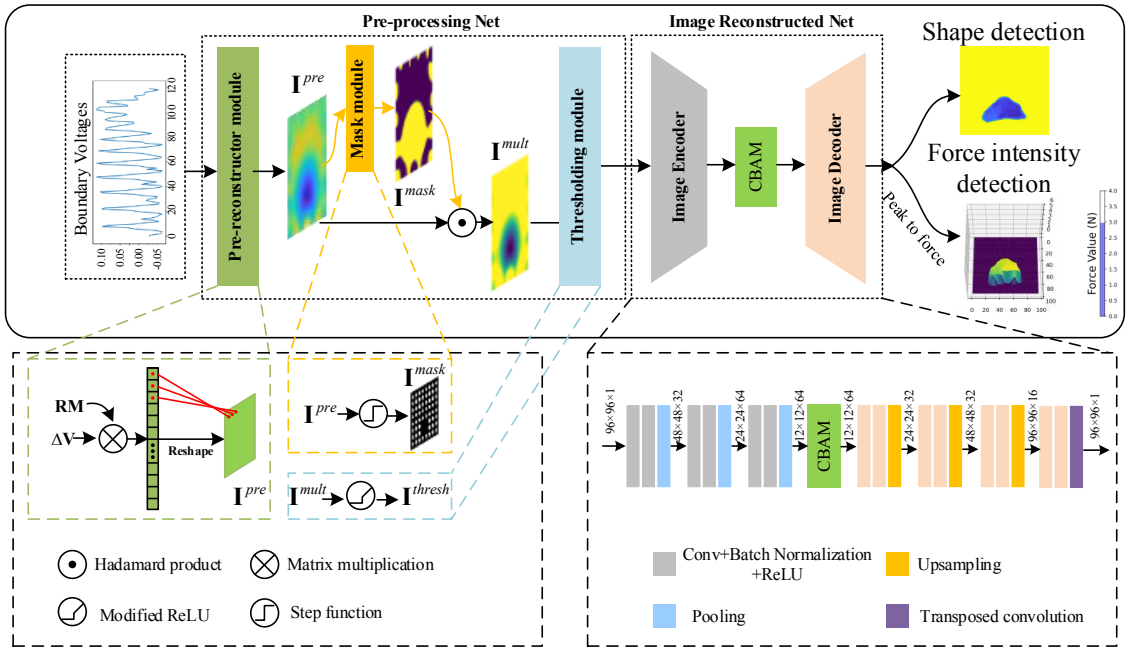

Fig. 1. (Top) An overview of MM-CNN network. (Bottom) The network architecture of MM-CNN network.

C. Tactile sensor fabrication

Figure 2 (a) shows the manufacturing process for the EIT sensor's materials. These comprise soft polyurethane foam, ionic liquid, Flexible Printed Circuit Board (FPCB), and Ecoflex. The FPCB forms the base while Ecoflex provides a flexible border, enabling conformation to uneven surfaces. The porous foam measures 10 mm × 10 mm × 5 mm. Sixteen electrodes evenly distributed on the FPCB provide connectivity. Construction involves placing the foam on the FPCB, filling with tap water as the ionic liquid, and sealing with an Ecoflex film to prevent leakage. The resulting sensor is depicted in Figure 2 (b).

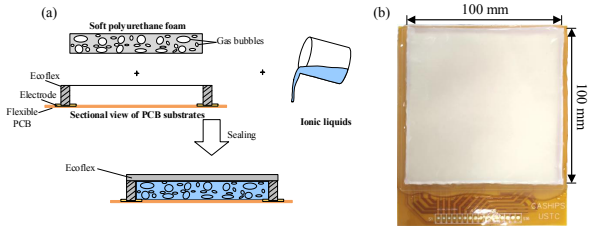

Fig. 2. Square tactile sensor. (a) Fabrication of flexible EIT-based tactile sensor.

D. Sensing system

A 16-electrode data acquisition circuit is designed (Figure 3). An AD5940 impedance measurement IC is used, capable of 0-200kHz signal generation and 200kHz bandwidth measurements [18]. A 40kHz excitation balances speed and accuracy, consistent with existing EIT systems [19], [20]. Four 16:1 multiplexers (ADG706) enable sequential electrode addressing. A 4-wire approach [18] measures impedance changes. This acquires 120 values from unique electrode pairs without repetition. A microcontroller (STM32) controls the multiplexers, coordinates the AD5940, and transfers data to a computer. Further implementation details are in our prior work [21].

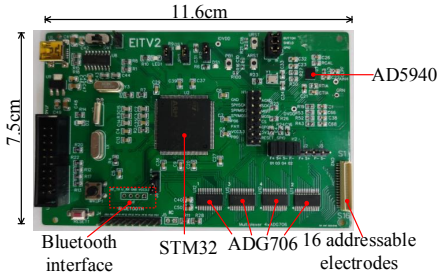

Fig. 3. The data acquisition board.

III. Simulation Studies

A. Training

Dataset generation: Numerical simulations were conducted using the open-source EIT toolkit EIDORS [22] to verify the touch detection efficacy of the MM-CNN tactile sensor. A square sensor model was constructed with a size of 2×2 and discretized into $96 \times 96 \times 2$ triangular finite elements. The current stimulus was set to 0.01 mA with a background conductivity of 1.0 S/m, and 16 sensing electrodes were evenly distributed around the boundary.

To simulate touch interactions, randomized conductivity perturbations were introduced, decreasing local values below the 1.0 S/m background. The disturbance region was assigned values ranging from 0.5-0.9 S/m, corresponding

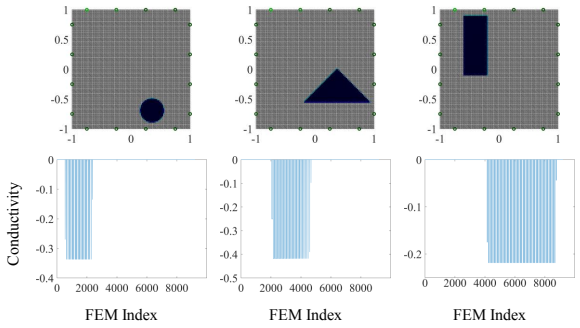

Fig. 4. Typical conductivity distribution samples with different shape targets and varied conductivity values.

to simulated touch forces of 5 N down to 1 N. Solving the forward model yielded corresponding sets of boundary voltages for each perturbation. In total, the dataset consisted of 8084 samples with five geometric touch shapes (circle, triangle, rectangle, square, L-shape) and varying conductivity levels. Figure 4 provides three representative conductivity distribution examples with different target shapes and values.

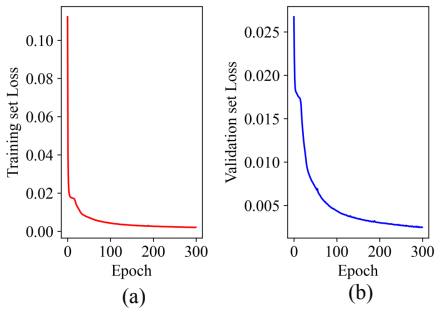

Fig. 5. (a) Loss curves of training set and (b) validation set against epoch during training.

Training Settings: For training, the input comprised the 120 boundary voltage measurements, while the output target was the associated 2D conductivity distribution. The MM-CNN model was implemented in Keras with a TensorFlow backend. The generated dataset was partitioned with a 90/10 split into training and validation sets respectively. A batch size of 64 was utilized. Optimization was performed using the ADAM algorithm with a learning rate of 0.00001. The model was trained for 300 epochs, showing convergence of the training error as depicted in Figure 5 (a). As observed in Figure 5 (b), the validation error closely tracked the training error throughout, without evidence of divergence.

B. Location-dependent performance test

To validate the proposed MM-CNN method for addressing the location-dependency problem in EIT, a simulation study was conducted using newly generated test data not present in the training set. As illustrated in Figure 6, 49 distinct touch locations were defined in a grid pattern over the sensing area. The grid consisted of a 7×7 array with 0.2 spacing, covering a 2×2 sensor. The locations were numbered left-to-right and top-to-bottom in a zig-zag order from 1 to

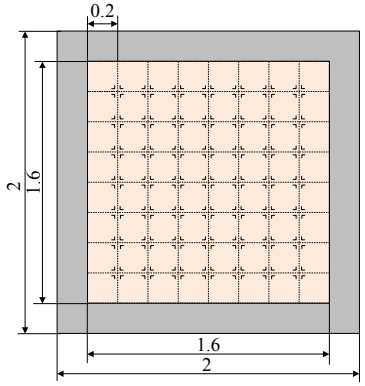

Fig. 6. 49 positions for single touch force test in the sensing area.

49. At each location, a circular touch perturbation with 0.2 radius and 0.15 S/m conductivity was applied to simulate localized contact. Reconstructions were then performed at all locations using the same contact patterns to evaluate algorithm performance across the sensor area.

For quantitative comparison, the reconstructed conductivity peaks were normalized to the value at the central position 25. Specifically, each reconstructed peak was divided by the peak magnitude at location 25. This normalized conductivity peak were computed from reconstructions generated separately using the proposed MM-CNN method, the NOSER linear algorithm, and the TV iterative algorithm. As depicted in Figure 7, the peak values from NOSER and TV exhibited substantial offsets from the true simulated conductivity across locations. In contrast, the normalized peaks from the MM-CNN method closely fluctuated around the target value.

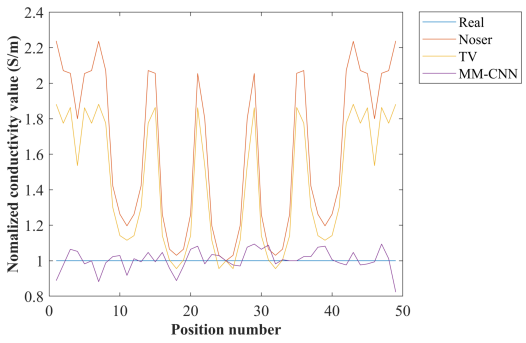

Fig. 7. Location-dependent test comparison.

To quantify the extent of location-dependent performance, we define a location-dependent consistency indicator (LDCI) as follow:

$$\mathrm{LDCI} = \frac{1}{P-1}\sum_{p=1}^{P}\left|\frac{pv_p^{(k)} - pv_{25}^{(k)}}{pv_{25}^{(k)}}\right| \tag{6}$$

where $pv_p^{(k)}$ represents the normalized reconstruction peak at position p, with the peak magnitude at the central sensor location p=25 used as the normalization reference. The superscript (k) indicates the reconstruction method, corresponding to MM-CNN, TV, and NOSER. To quantify

spatial accuracy, the LDCI metric was calculated for each method. Lower LDCI indicates more uniform sensitivity, with 0 representing perfect uniformity. The proposed MM-CNN achieved the minimum LDCI of 0.04, compared to 0.45 for TV and 0.60 for NOSER. These results demonstrate that the proposed method can effectively reduce the location dependency inherent to EIT, providing the potential for more precise force detection using EIT-based tactile sensors.

IV. Tactile Sensor Experiment

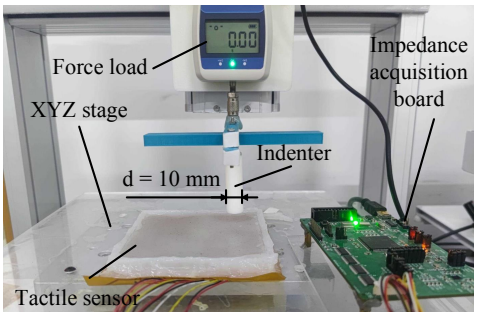

Fig. 8. Experimental apparatus for evaluating the tactile sensor performance.

Indentation experiments were conducted to evaluate the force detection capabilities of the proposed MM-CNN method using a flexible EIT-based tactile sensor. As depicted in Figure 8, an experimental apparatus was developed for controlled indentation across the sensor area. The tactile sensor was fixed horizontally while an indenter with a 10 mm diameter was mounted to a computer-controlled XYZ stage programmed to move vertically (z-axis) for indentation. An inline commercial force gauge (SH-100, NSCING, China) applied precise indentation forces.

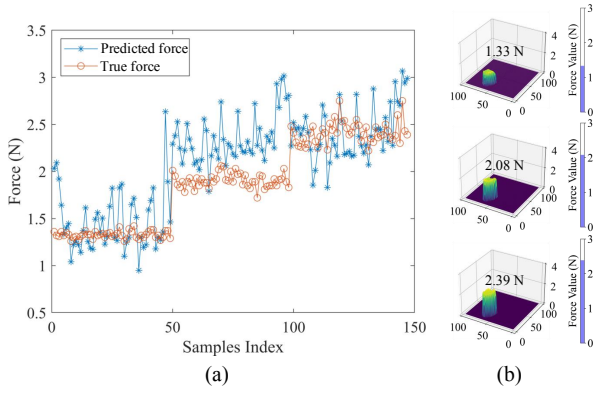

Fig. 9. Force estimation test. (a) Force estimation results. (b)Three representive reconstructed images under different forces.

Testing was conducted at 49 locations matching the grid layout (Figure 6). Approximately equivalent forces were applied at each position and the true applied force value was recorded by the commercial force gauge. The impedance acquisition system measured boundary voltages during indentation, which were input to the MM-CNN model for image reconstruction. As established through simulations, the 0.5-0.9 S/m conductivity range corresponds to 1-5 N forces. Thus, the reconstructed conductivity peaks were directly converted to force estimates without calibration.

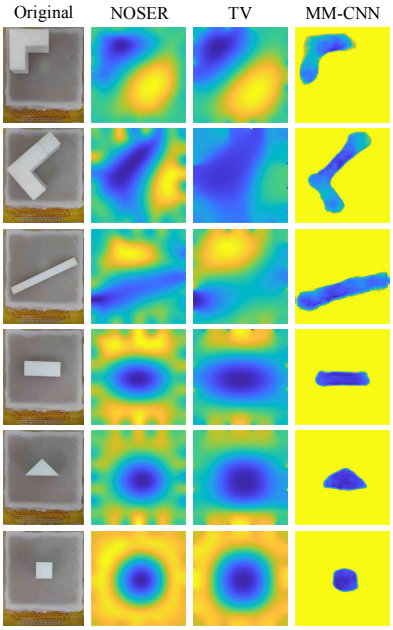

Fig. 10. The results of contact detection experiments.

Figure 9 (a) depicts the force values predicted by the MM-CNN model compared to distinct applied indentation forces at different sensor locations. Additionally, Figure 9 (b) presents reconstructed images generated by the MM-CNN model for three distinct indentation forces, demonstrating the model's force visualization capabilities. Overall, the MM-CNN achieved a 16.62% force estimation error across all experimental trials. It should be noted that the network parameters utilized for both the force and shape detection experiments were directly derived from training on the aforementioned simulated datasets, without additional tuning on real sensor data.

The generalized shape reconstruction capabilities were examined by testing several complex tactile stimuli on the real sensor. Figure 10 presents the reconstructions for selected measurement scenarios. The first column depicts the experimental recordings obtained by pressing different objects onto the sensor, including L-shape, rectangular, triangular, and square contact regions. Comparing the three reconstruction methods, NOSER and TV could partially capture the impedance change area location, while the proposed MM-CNN more accurately reconstructed the precise shape. Additionally, NOSER and TV struggled to distinguish between small shapes like triangles and squares, whereas MM-CNN reliably differentiated them.

To quantitatively evaluate the reconstruction performance, we implemented the Mean Intersection over Union (MIoU) metric to compare the real contact region and reconstructed impedance distribution:

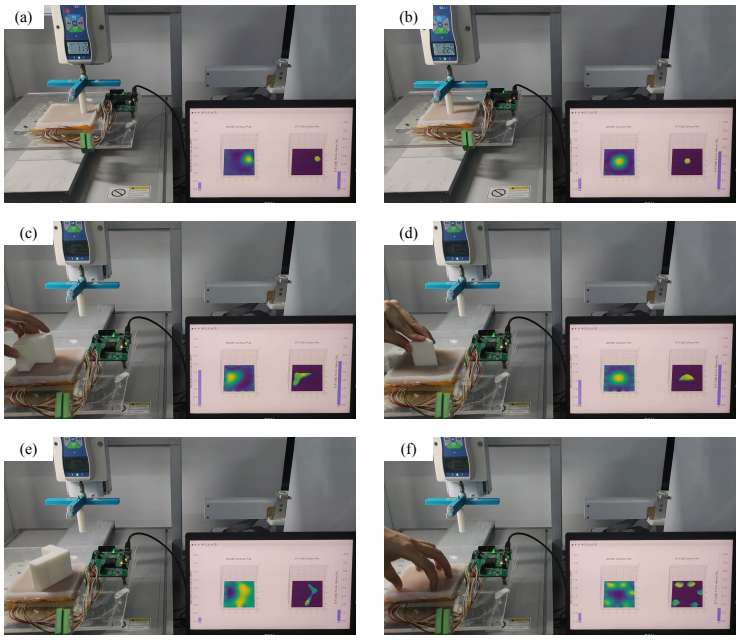

Fig. 11. Performance comparison of three reconstruction algorithms in contact shape detection experiment.

$$\mathrm{MIoU} = \frac{1}{k+1}\sum_{i=0}^{k}\frac{p_{ii}}{\sum_{j=0}^{k}p_{ij} + \sum_{j=0}^{k}p_{ij} - p_{ii}} \tag{7}$$

where k represents the number of classes and p_{ij} denotes the number of pixels of class i predicted as belonging to class j. Higher MIoU values indicate improved performance, with a maximum MIoU of 1 corresponding to perfect reconstruction.

The MIoU was averaged over six representative contact cases. The Noser method obtained an average MIoU of 0.36, the TV algorithm achieved 0.30, while the proposed MM-CNN method attained the highest score of 0.69. This superior MIoU demonstrates the MM-CNN enables accurate shape detection with the tactile sensor system.

Figure 11 presents examples of real-time touch detection using the proposed MM-CNN method on a flexible EIT-based tactile sensor (see Supplementary Video 1). Figures 11 (a) and 11 (b) demonstrate force detection capabilities. An indentation apparatus with integrated commercial force gauge (SH-100, NSCING, China) was utilized to precisely apply forces at specified locations. The corresponding 3D reconstructed images are displayed for both the NOSER algorithm (left) and MM-CNN (right). Adjacent force bars indicate the predicted force from each method. As indentation force rises, the image height increases accordingly, along with the force bar values. The results showcase the MM-CNN's improved accuracy by compensating for EIT's inherent location-dependency.

Figures 11 (c)- 11 (d) showcase shape detection for four representative objects. When objects with various profiles are placed anywhere on the sensor, their shape can be effectively identified, with intensity reflected by the force bar. Additionally, the proposed MM-CNN approach enables multi-point touch detection.

V. CONCLUSION

In this work, we achieve simultaneous contact force and shape detection using a flexible EIT-based tactile sensor. The proposed model-driven multimodal convolutional neural network (MM-CNN) integrates physics-based preprocessing with a learning-based reconstruction network, synergistically combining analytical and data-driven approaches. Critically, the model trained purely on simulated data successfully generalizes to multi-contact experiments on the real sensor. Numerical and experimental validations demonstrate the efficacy of the method. Across varied indentation trials, the sensor achieved a 16.62% force estimation error. Additionally, the sensor achieved accurate reconstruction and identification of at least six distinct contact shapes along with multi-point touch capabilities.

ACKNOWLEDGMENT

This work was supported in part by the National Natural Science Foundation of China (Grant No.62303436); in part by the Open Project of Anhui Provincial Key Laboratory of Infrared and Low Temperature Plasma (Grant No. IRKL2022KF04); in part by special key project of technological innovation and application development in Chongqing (Grant No. CSTB2022TIAD-KPX0134).

REFERENCES

[1] G. Li, S. Liu, Q. Mao, and R. Zhu, "Multifunctional electronic skins enable robots to safely and dexterously interact with human," *Advanced Science*, vol. 9, no. 11, p. 2104969, 2022.

[2] G. Pang, G. Yang, and Z. Pang, "Review of robot skin: A potential enabler for safe collaboration, immersive teleoperation, and affective interaction of future collaborative robots," *IEEE Transactions on Medical Robotics and Bionics*, vol. 3, no. 3, pp. 681–700, 2021.

[3] Z. V. Gbouna, G. Pang, G. Yang, Z. Hou, H. Lv, Z. Yu, and Z. Pang, "User-interactive robot skin with large-area scalability for safer and natural human-robot collaboration in future telehealthcare," *IEEE journal of biomedical and health informatics*, vol. 25, no. 12, pp. 4276–4288, 2021.

[4] R. Dahiya, N. Yogeswaran, F. Liu, L. Manjakkal, E. Burdet, V. Hayward, and H. Jörntell, "Large-area soft e-skin: The challenges beyond sensor designs," *Proceedings of the IEEE*, vol. 107, no. 10, pp. 2016–2033, 2019.

[5] D. Silvera-Tawil, D. Rye, M. Soleimani, and M. Velonaki, "Electrical impedance tomography for artificial sensitive robotic skin:a review," *IEEE Sensors Journal*, vol. 15, no. 4, pp. 2001–2016, 2015.

[6] K. Park, H. Yuk, M. Yang, J. Cho, H. Lee, and J. Kim, "A biomimetic elastomeric robot skin using electrical impedance and acoustic tomography for tactile sensing," *Science Robotics*, vol. 7, no. 67, p. eabm7187, 2022.

[7] D. S. Holder, *Electrical Impedance Tomography : Methods, History and Applications*. Bristol, U.K.: IOP Publishing, 2005.

[8] Y. Chen and H. Liu, "Location-dependent performance of large-area piezoresistive tactile sensors based on electrical impedance tomography," *IEEE Sensors Journal*, vol. 21, no. 19, pp. 21 622–21 630, 2021.

[9] M. Cheney, D. Isaacson, J. C. Newell, S. Simske, and J. Goble, "Noser: An algorithm for solving the inverse conductivity problem," *International Journal of Imaging systems and technology*, vol. 2, no. 2, pp. 66–75, 1990.

[10] A. Borsic, B. M. Graham, A. Adler, and W. R. Lionheart, "In vivo impedance imaging with total variation regularization," *IEEE transactions on medical imaging*, vol. 29, no. 1, pp. 44–54, 2009.

[11] Z. Husain, N. A. Madjid, and P. Liatsis, "Tactile sensing using machine learning-driven electrical impedance tomography," *IEEE Sensors Journal*, vol. 21, no. 10, pp. 11 628–11 642, 2021.

[12] H. Park, K. Park, S. Mo, and J. Kim, "Deep neural network based electrical impedance tomographic sensing methodology for large-area robotic tactile sensing," *IEEE Transactions on Robotics*, vol. 37, no. 5, pp. 1–14, 2021.

[13] H. Lee, H. Sun, H. Park, G. Serhat, B. Javot, G. Martius, and K. J. Kuchenbecker, "Predicting the force map of an ert-based tactile sensor using simulation and deep networks," *IEEE Transactions on Automation Science and Engineering*, vol. 20, no. 1, pp. 425–439, 2022.

[14] A. Adler, J. Arnold, R. Bayford, A. Borsic, B. Brown, P. Dixon, T. Faes, I. Frerichs, H. Gagnon, and Y. Garber, "Greit: a unified approach to 2d linear eit reconstruction of lung images," *Physiological Measurement*, vol. 30, no. 6, pp. S35–55, 2009.

[15] A. Adler, T. Dai, and W. R. Lionheart, "Temporal image reconstruction in electrical impedance tomography," *Physiological measurement*, vol. 28, no. 7, p. S1, 2007.

[16] H. Chen, X. Yang, J. Geng, G. Ma, and X. Wang, "A convolutional neural network based electrical impedance tomography method for skin-like hydrogel sensing," in *2022 IEEE International Conference on Robotics and Biomimetics (ROBIO)*, 2022, pp. 178–183.

[17] S. Woo, J. Park, J.-Y. Lee, and I. S. Kweon, "Cbam: Convolutional block attention module," in *Proceedings of the European conference on computer vision (ECCV)*, 2018, pp. 3–19.

[18] Analog Devices, High Precision, Impedance, and Electrochemical Front End AD5940/5941, Data Sheet. Accessed: 2020. [Online]. Available: https://www.analog.com/media/en/technical-documentation/data-sheets/AD5940-5941.pdf.

[19] G. Ma, Z. Hao, X. Wu, and X. Wang, "An optimal electrical impedance tomography drive pattern for human-computer interaction applications," *IEEE Transactions on Biomedical Circuits and Systems*, vol. 14, no. 3, pp. 402–411, 2020.

[20] Y. Zhang, R. Xiao, and C. Harrison, "Advancing hand gesture recognition with high resolution electrical impedance tomography," in *Proceedings of the 29th Annual Symposium on User Interface Software and Technology*. ACM, 2016, pp. 843–850.

[21] H. Chen, X. Yang, P. Wang, J. Geng, G. Ma, and X. Wang, "A large-area flexible tactile sensor for multi-touch and force detection using electrical impedance tomography," *IEEE Sensors Journal*, vol. 22, no. 7, pp. 7119–7129, 2022.

[22] A. Adler and W. R. Lionheart, "Uses and abuses of eidors: an extensible software base for eit," *Physiological measurement*, vol. 27, no. 5, pp. S25–S42, 2006.